Quantitative measurement of the orbital angular momentum density of light

Angela Dudley,[1,2] Igor A. Litvin,[1] and Andrew Forbes[1,2,*]

[1]Council for Scientific and Industrial Research National Laser Centre, P.O. Box 395, Pretoria 0001, South Africa

[2]School of Physics, University of KwaZulu-Natal, Private Bag X54001, Durban 4000, South Africa

*Corresponding author: aforbes1@csir.co.za

Received 23 September 2011; accepted 15 November 2011;
posted 18 November 2011 (Doc. ID 155256); published 23 February 2012

In this work we derive expressions for the orbital angular momentum (OAM) density of light, for both symmetric and nonsymmetric optical fields, that allow a direct comparison between theory and experiment. We present a simple method for measuring the OAM density in optical fields and test the approach on superimposed nondiffracting higher-order Bessel beams. The measurement technique makes use of a single spatial light modulator and a Fourier transforming lens to measure the OAM spectrum of the optical field. Quantitative values for the OAM density as a function of the radial position in the optical field are obtained for both symmetric and nonsymmetric superpositions, illustrating good agreement with the theoretical prediction.

OCIS codes: 090.1995, 120.4570, 070.6120, 070.3185, 050.4865.

1. Introduction

Since the discovery of optical fields carrying orbital angular momentum (OAM) [1], many new avenues in the field of classical and quantum optics have been initiated, ranging from the transfer of OAM to particles in optical tweezers [2] to the entanglement of OAM in parametric downconversion [3]. Fields that carry OAM of $l\hbar$ per photon, some of which include Laguerre–Gaussian beams [4], Bessel–Gaussian beams [5], and Airy beams [6], have an azimuthal angular dependence of $\exp(il\phi)$ [1,4], where l is the unbounded azimuthal mode index and ϕ is the azimuthal angle. Since these fields possessing OAM offer an unbounded state space, they provide a larger bandwidth for quantum cryptography [7–9], leading to many publications being dedicated to the measurement of OAM in order for higher-dimensional quantum information processing to be a success.

Many techniques exist in the area of measuring OAM, from computer generated holograms [3,10–12] to interferometers [13–15]. Even though the aforementioned techniques are efficient at sorting modes (and even in some cases single photons) carrying OAM, they do not allow one to obtain a quantitative measurement for the OAM density and instead only measure the global OAM—the average value across the entire field. In the last year, more techniques that measure the global OAM have appeared, from demultiplexing free-space OAM-carrying beams [16] to studying the diffraction patterns of helical beams [17]. Many publications demonstrate the transfer of local OAM to trapped particles [18–20] by illustrating that the rotation rates of a particle trapped at different radial positions in a multiringed beam are proportional to r^{-3} [18], or by illustrating that particles trapped at different radial positions in an optical field (produced by interfering two vortex beams with unequal charges) rotate in opposite directions [20]. The only attempts, to the best of our knowledge, to make quantitative measurements of the OAM carried in an optical field have been made by merely measuring these rotation rates [21,22]. Measuring OAM by demonstrating rotation within an optical tweezing system is not only

1559-128X/12/070823-11$15.00/0

an indirect measurement but also a difficult experiment to conduct. The results of these findings only illustrate that the rotation rates reveal that the transferred angular momentum increases linearly with laser power [21] and that the rotation rates of low-index particles, which locate themselves in the dark regions of optical fields, are not impeded by beam imperfections [22]. Another, even more complicated, technique makes use of Doppler shifts due to a rotating detector [23,24], which allows for the reconstruction of the OAM spectrum of an optical field and has been tested with Laguerre–Gaussian modes of different azimuthal orders [23].

In this paper we present a technique for a simple and direct measurement of the OAM density that requires only a spatial light modulator (SLM) and a lens. Having a tool to perform a quantitative measurement of the OAM density will prove useful not only in quantum information but also in determining the loss in angular momentum as optical vortices breakup during nonlinear propagation [25]. We formulate the theoretical equation for the OAM density for both symmetric and nonsymmetric fields and use the Fresnel diffraction integral to formulate an experimental form for the OAM density, allowing for the first time (to our knowledge) a quantitative measurement of the OAM density of the field. We implement this simple experimental technique to obtain quantitative measurements for the OAM density for both symmetric and nonsymmetric superpositions of nondiffracting higher-order Bessel beams.

2. Concept of the OAM Density Measurement

In this section we investigate how the OAM density of an optical field can be measured. An illustration that will aid the theoretical description, as well as the experimental measurement, of the OAM density is given in Fig. 1(a). Figure 1(a), which denotes a schematic of the experimental setup for the OAM density measurement, is separated into two parts: (1) the generation of the optical field and (2) the measurement of the OAM density, which is achieved by performing a modal decomposition of the optical field.

A. Symmetric Superposition of Two Bessel Beams

In this paper, we use Bessel beams as a basis set for OAM-carrying fields and classify the superpositions of nondiffracting higher-order Bessel beams into symmetric and nonsymmetric. In our derivation of both the theoretical and experimental OAM densities, we will start with the symmetric case and later develop the argument for the nonsymmetric case. Consider the amplitude for a symmetric superposition of two Bessel beams, of opposite azimuthal order, as given by

$$u(r,\theta,z) = A_0(J_l(q_1 r)\exp(i\Delta k z)\exp(il\theta) + \alpha_0 J_{-l}(q_2 r)\exp(-i\Delta k z)\exp(-il\theta)), \quad (1)$$

where J_l and J_{-l} denote the Bessel functions of order l and $-l$, respectively, q_1 and q_2 denote the radial wavenumbers of the two fields, and Δk denotes the difference between the longitudinal wavenumbers. We start with this special case, as the theoretical OAM density is already known [26].

To experimentally create such a field, Durnin's ring slit [27] method is used; however the ring slit is encoded digitally [28] onto an SLM. By dividing the ring slit into two ring slits and encoding the azimuthal phase within the ring slits to vary azimuthally in opposite directions, a superposition of two oppositely handed Bessel beams can be generated. For the example given in Fig. 1(c), the phase within the inner ring slit varies three times in a clockwise

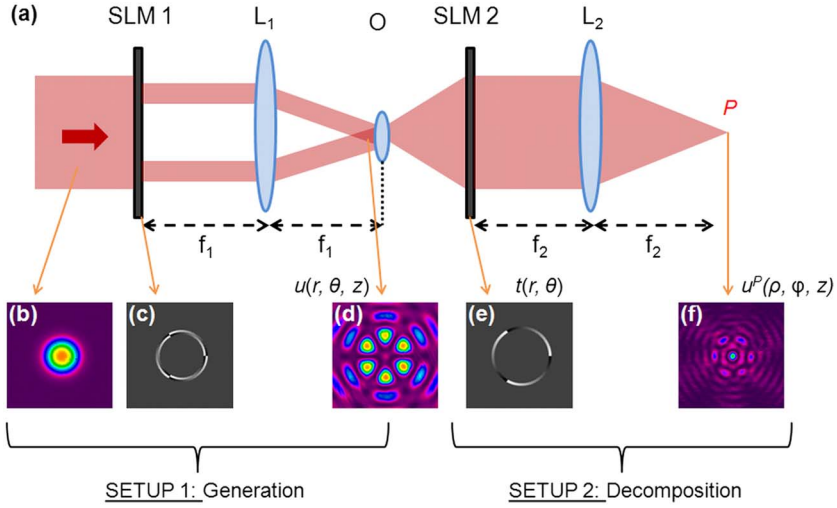

Fig. 1. (Color online) (a) Schematic of the concept for generating the optical field and decomposing its OAM spectrum. (b) The Gaussian beam used to illuminate (c) the digital ring slit hologram for the construction of (d) the optical field, mathematically defined by $u(r,\theta,z)$. (e) The hologram, having a transmission function of $t(r,\theta)$, together with the lens L_2, performs the decomposition, which produces (f) the inner product at plane P, mathematically defined by $u^P(0,\phi,z)$. SLM, spatial light modulator; O, objective—used to magnify the optical field (d).

direction ($l = 3$), and three times in a counterclockwise direction ($l = -3$) in the outer ring slit, thus transforming the initial Gaussian beam [Fig. 1(b)] into a superposition of two Bessel beams, of orders $l = 3$ and -3, denoted by the "petal" structure [Fig. 1(d)].

The widths of the two ring slits can be adjusted, consequently increasing or decreasing the energy present in the two Bessel beams. The energy contained within the first Bessel beam, J_l, is denoted by A_0 in Eq. (1), and the energy contained within the second Bessel beam, J_{-l}, is denoted by $\alpha_0 A_0$, with the constants determined as

$$A_0 = \sqrt{\int_{\text{ring1}} \exp(-2(r/\omega)^2) r \mathrm{d}r}, \tag{2}$$

$$\alpha_0 = \sqrt{\int_{\text{ring2}} \exp(-2(r/\omega)^2) r \mathrm{d}r \Big/ \int_{\text{ring1}} \exp(-2(r/\omega)^2) r \mathrm{d}r}, \tag{3}$$

where ring1 and ring2 denote the bounds of the inner and outer radii for the inner and outer rings, respectively, and ω is the radius of the Gaussian beam illuminating the ring slit.

In determining a theoretical equation for the OAM density, the Poynting vector for the optical field [Eq. (1)] needs to be solved:

$$\vec{S} = \frac{\varepsilon_0 \omega c^2}{4} (i(u \nabla u^* - u^* \nabla u) + 2\, k |u|^2 \hat{z}), \tag{4}$$

where ε_0 is the permittivity of free space, c is the speed of light, k is the wavenumber, and u is the amplitude of the field described in Eq. (1). The OAM density, L_z, can then be determined from the Poynting vector by the following relationship:

$$L_z = \frac{1}{c^2} (\vec{r} \times \vec{S})_z, \tag{5}$$

resulting in [26]

$$L_z^{\text{THEORY}}(r) = \frac{l \varepsilon_0 \omega A_0^2}{2} (J_l^2(q_1 r) + \alpha_0^2 J_{-l}^2(q_2 r)), \tag{6}$$

the theoretical description of the OAM density for the symmetric superposition described in Eq. (1).

Once the optical field is generated, a quantitative measurement of the OAM density, given theoretically in Eq. (6), can be made by measuring the weighting of each azimuthal mode present in the optical field, which is done by performing the following inner product [depicted in the decomposition section of Fig. 1(a)]:

$$a_n(r, z) = \frac{1}{\sqrt{2\pi}} \int_0^{2\pi} u(r, \theta, z) t(r, \theta) \mathrm{d}\theta. \tag{7}$$

a_n is the weighting of the azimuthal mode of order n present in the optical field $u(r, \theta, z)$, described by Eq. (1), and $t(r, \theta)$, which is the transmission function of SLM 2 in Fig. 1(a) and is termed the match filter, is given by the azimuthal mode, $\exp(-in\theta)$, within the bounds $R_1 < r < R_2$. The concept of using a match filter to detect predetermined signals within a noisy background was first demonstrated nearly 50 years ago [29]. This involved implementing complex spatial filters recorded onto film to identify geometric shapes, letters, and signals within random noise. The inner product is executed experimentally by directing the optical field, $u(r, \theta, z)$, onto a match filter [encoded on an SLM and denoted in Fig. 1(e)] and viewing the Fourier transform [depicted in Fig. 1(f)]. The match filter, an example of which is given in Fig. 1(e), consists of a ring slit placed at a particular radial position (R), which allows one to select the radial position within the optical field. The azimuthal phase within the ring slit varies as $\exp(-in\theta)$. For this particular example [Fig. 1(e)], the weighting of the azimuthal mode, $n = 3$ (i.e., a_3), is being measured. By adjusting the azimuthal phase within the ring slit and the radius of the ring slit, various azimuthal weightings at different radial positions in the optical field can be measured. This technique is not restricted to superpositions of Bessel beams but can be used on any OAM-carrying optical field.

To relate the weighting of the azimuthal mode to a quantitative laboratory measurement, we require the inner product of u and t to be determined. The inner product [located at plane P in Fig. 1(a) and defined as $u^P(0, \phi, z)$] is determined by making use of the Fresnel diffraction integral to propagate the field from SLM 2 [the initial field, $u(r, \theta, z)$, multiplied by the transmission function, $t(r, \theta)$, of the match filter] to plane P (the plane of the inner product):

$$u^P(\rho, \phi, z) = \frac{\exp(i2kf)}{i\lambda f} \int_0^{\infty} \int_0^{2\pi} t(r, \theta) u(r, \theta, z) \times \exp\left(-i \frac{k}{f} r\rho \cos(\theta - \phi)\right) r \mathrm{d}r \mathrm{d}\theta, \tag{8}$$

where f is the focal length of the lens used in the decomposition.

If Eq. (8) is evaluated at the origin, $\rho = 0$, then we return the desired inner product between the field $u(r, \theta, z)$ and the match filter $t(r, \theta)$. We also know that when the match filter consists of the complex conjugate of one of the azimuthal modes present in the initial field, the weighting of the azimuthal mode, a_n, [or the on-axis intensity of the inner product, $I(\rho = 0)$] will be nonzero; therefore, we need only consider the cases when the azimuthal mode of the match filter is either l or $-l$ (i.e., $n = l$ and $-l$). By substituting Eq. (1) into Eq. (8), and considering the signal at the origin, $u^P(0, \phi, z)$, for cases when the azimuthal mode index of the match filter is either l or $-l$, we find, respectively,

$$u_l^p(\rho=0,z)=\frac{\exp(i2kf)}{i\lambda f}2\pi A_0\int_{R_1}^{R_2}J_l(q_1r)\times\exp(i\Delta kz)r\mathrm{d}r, \tag{9}$$

$$u_{-l}^P(\rho=0,z)=\frac{\exp(i2kf)}{i\lambda f}2\pi A_0\alpha_0\int_{R_1}^{R_2}J_{-l}(q_2r)\times\exp(-i\Delta kz)r\mathrm{d}r. \tag{10}$$

R_1 and R_2 are the inner and outer radii of the ring slit representing the match filter [Fig. 1(e)]. Since the ring slit in the match filter can be made arbitrarily thin, Eqs. (9) and (10) can be simplified by noting that the ring slit may be assumed to be at a radial position $R\approx R_1\approx R_2$ and of width $2\Delta R$, resulting in

$$u_l^p(\rho=0,z,r=R)=\frac{\exp(i2kf)}{i\lambda f}2\pi A_0 2\Delta R\cdot RJ_l(q_1R)\exp(i\Delta kz), \tag{11}$$

$$u_{-l}^P(\rho=0,z,r=R)=\frac{\exp(i2kf)}{i\lambda f}2\pi A_0\alpha_0 2\Delta R\cdot RJ_{-l}(q_2R)\exp(-i\Delta kz). \tag{12}$$

The Bessel function is evaluated at R, which is the radius of the ring slit, represented in the match filter.

Since the intensity of an optical field is defined as $I_l=\varepsilon_0 c(u_l u_l^*)$, the following relationships between the measured intensity at the origin of the inner product, $I(0)$ (for the two cases where the azimuthal mode index of the match filter is either l or $-l$), and the theoretical Bessel functions can be formed:

$$\frac{I_l(0)}{\varepsilon_0 c}\left(\frac{f\lambda}{4\pi\Delta R\cdot RA_0}\right)^2=J_l^2(q_1R), \tag{13}$$

$$\frac{I_{-l}(0)}{\varepsilon_0 c}\left(\frac{f\lambda}{4\pi\Delta R\cdot RA_0}\right)^2=\alpha_0^2J_{-l}^2(q_2R). \tag{14}$$

Substituting the above two equations, Eqs. (13) and (14), for the Bessel functions, J_l and J_{-l}, into the theoretical result for the OAM density, Eq. (6), results in the following equation:

$$L_z^{\mathrm{EXP}}(R)=\frac{l\omega}{2\,c\eta}\left(\frac{\lambda f}{S_{\mathrm{Ring}}}\right)^2(I_l(0)-I_{-l}(0)), \tag{15}$$

which is used to calculate quantitative measurements of the OAM density. η is a factor for the optical efficiency of the experimental setup, and S_{Ring} is the area $(4\pi\Delta R\cdot R)$ of the ring slit in the match filter and is a function of its radial position, R.

B. Generalized Symmetric Superposition

The optical field for which we wish to measure the OAM density, as described in Eq. (1), can be extended to a generalized form:

$$u(r,\theta,z)=A_0\sum_{l=-N}^{N}\alpha_l J_l(q_lr)\exp(i\Delta k_l z)\exp(il\theta)+\alpha_{-l}J_{-l}(q_{-l}r)\exp(-i\Delta k_{-l}z)\exp(-il\theta), \tag{16}$$

where α_l and α_{-l} denote the energy contained in each of the ring slits with respect to the energy contained in the innermost ring slit. Because of the fact that the ϕ-component of the Poynting vector, S_ϕ, is a linear operator (the proof is contained in detail in Appendix A), the OAM density for the generalized field described in Eq. (16) can be described both theoretically and experimentally by extending the results given in Eqs. (6) and (15) as, respectively,

$$L_z^{\mathrm{THEORY}}(r)=\frac{\varepsilon_0\omega A_0^2}{2}\sum_{l=-N}^{N}l\alpha_l^2J_l^2(q_lr)-l\alpha_{-l}^2J_{-l}^2(q_{-l}r), \tag{17}$$

$$L_z^{\mathrm{EXP}}(R)=\frac{\omega}{2\,c\eta}\left(\frac{\lambda f}{S_{\mathrm{Ring}}}\right)^2\sum_{l=-N}^{N}l(I_l(0)-I_{-l}(0)). \tag{18}$$

C. Nonsymmetric Superposition of Two Bessel Beams

The other case that is investigated in this paper is that of nonsymmetric superpositions of Bessel beams, and in the following equations we will outline the theoretical analysis for obtaining the OAM density. The amplitude of a nonsymmetric superposition of two Bessel beams can be described as

$$u(r,\theta,z)=A_0(J_l(q_1r)\exp(i\Delta kz)\exp(il\theta)+\alpha_0J_m(q_2r)\exp(-i\Delta kz)\exp(im\theta)), \tag{19}$$

where the azimuthal indices are of different orders, $l\neq m$. Following the same procedure in determining the Poynting vector and consequently the OAM density previously described for the symmetric case [Eqs. (4) and (5)], the OAM density is determined theoretically by

$$L_z^{\mathrm{THEORY}}(r,\phi,z)=\frac{\varepsilon_0\omega A_0^2}{2}(lJ_l^2(q_1r)+m\alpha_0^2J_m^2(q_2r)+(l+m)\alpha_0\cos((l-m)\phi+2\Delta kz)J_l(q_1r)J_m(q_2r)). \tag{20}$$

Since the above equation is a function of the azimuthal angle, ϕ, in the plane of the inner product, it is evaluated by summing the OAM density values for a range of angles varying from 0 to 2π.

Equation (20), unlike the OAM density for the symmetric case, is a function of Δkz, and given that its effect on the optical field is only a constant phase shift (a rotation in the intensity profile of the optical field), it can be ignored.

To relate a quantifiable measurement to the theoretical OAM density [Eq. (20)], the same procedure as described in Eqs. (8)–(14) is followed, and the final results, which relate the on-axis intensity in the inner product plane P to the theoretical Bessel functions, are

$$\frac{I_l(0)}{\varepsilon_0 c}\left(\frac{f\lambda}{4\pi\Delta R\cdot RA_0}\right)^2 = J_l^2(q_1R), \tag{21}$$

$$\frac{I_m(0)}{\varepsilon_0 c}\left(\frac{f\lambda}{4\pi\Delta R\cdot RA_0}\right)^2 = \alpha_0^2 J_m^2(q_2R). \tag{22}$$

Here in the theoretical analysis of the nonsymmetric case, the azimuthal mode index, n, of the match filter is set to both l and m.

Substituting the above two equations, Eqs. (21) and (22), into Eq. (20), the form for obtaining an experimental measurement of the OAM density is

$$L_z^{\mathrm{EXP}}(R,\phi,z) = \frac{\omega}{2c\eta}\left(\frac{\lambda f}{S_{\mathrm{Ring}}}\right)^2\Big(lI_l(0) + mI_m(0) + (l+m)\cos((l-m)\phi + 2\Delta kz)\sqrt{I_l(0)}\sqrt{I_m(0)}\Big). \tag{23}$$

This result is also a function of the angle, ϕ, in the plane of the inner product, and since only a single measurement of the on-axis intensity in the inner product plane can be made, no measurement for the angle ϕ can be obtained. To resolve this issue, the experimental equation for the OAM density is integrated over ϕ, resulting in the average OAM density

$$\overline{L_z^{\mathrm{EXP}}(R)} = \frac{\omega}{2c\eta}\left(\frac{\lambda f}{S_{\mathrm{Ring}}}\right)^2(lI_l(0) + mI_m(0)), \tag{24}$$

where the term Δkz can be neglected. Since the above experimental measurement, Eq. (24), has no angular dependence on the optical field, the measurement does not pertain to a specific radial direction but is in fact merely an average measurement across the field.

D. Generalized Nonsymmetric Superposition

Similarly, as in the symmetric case, the amplitude of the nonsymmetric superposition can be extended to consist of many Bessel beams, as in the following form:

$$u(r,\theta,z) = A_0\sum_{l=-N}^{N}\sum_{m=-N}^{N}\alpha_l J_l(q_l r)\exp(i\Delta k_l z)\exp(il\theta) + \alpha_m J_m(q_m r)\exp(i\Delta k_m z)\exp(im\theta). \tag{25}$$

Even though the ϕ-component of the Poynting vector, S_ϕ, is a linear operator and the theoretical and experimental OAM densities can be extracted by extending the simple form in Eqs. (20) and (23), the equations become very cumbersome and have thus been neglected in this paper. However, if the reader wishes to calculate the OAM density for such fields, this can be easily achieved by substituting the amplitude of the field into Eq. (4) to determine the Poynting vector for calculating the theoretical OAM density.

In this paper we experimentally test the results given above by measuring the OAM density for six separate optical fields. The first three fields consist of a superposition of two Bessel beams, of orders 3 and −3, where (1) the energy in the two ring slits (used to generate the optical fields) is equal, (2) that in the outer ring slit is heavily weighted, and (3) that in the inner ring slit is heavily weighted. The theoretical and experimental OAM densities are calculated through the use of Eqs. (6) and (15). The fourth optical field is a nonsymmetric superposition of two Bessel beams, where $l = 3$ and $m = -4$, and the required results are obtained through the use of Eqs. (20) and (24). The fifth involves a superposition of three Bessel beams, and even though the OAM density is not explicitly given in the paper, it is easily calculated by substituting the amplitude of the optical field into Eqs. (4) and (5). This is also the case with the last optical field, a nonsymmetric superposition of four Bessel beams.

The experimental setup for measuring the OAM density of the optical fields, discussed above, is given in the following section, accompanied with the theoretical and experimental results.

3. Experimental Methodology and Results

The experimental setup for the measurement of the OAM spectrum at specific radial positions for the coherent superposition of Bessel beams is denoted in Fig. 2. To generate the various superimposed Bessel beams, for which we intend to calculate the OAM density, a HeNe laser ($\lambda \sim 633$ nm) was expanded through a 6× telescope and directed onto the liquid-crystal display (LCD) of an SLM labeled LCD_1. The fields consisting of superpositions of higher-order Bessel beams were generated in a similar approach to Durnin's ring slit [27] method, except the ring slits were implemented digitally [28] onto LCD_1 (HoloEye, PLUTO-VIS, with 1920 × 1080 pixels of pitch 8 μm and calibrated for a 2π phase shift at ~633 nm).

Some of the digital ring slit holograms programmed onto LCD_1 for the creation of superimposed Bessel beams are given in the first column of Fig. 3. To create an amplitude ring slit digitally on a phase-only SLM, the area surrounding the ring

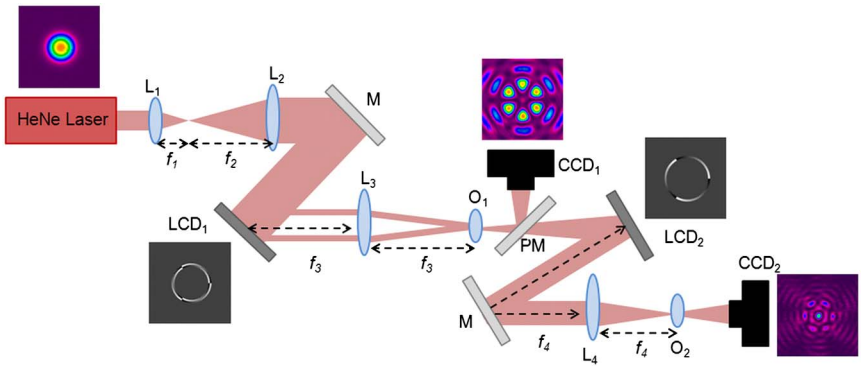

Fig. 2. (Color online) Schematic of the experimental setup for measuring the OAM density of symmetric and nonsymmetric superpositions of Bessel beams as a function of the radial position, R. L, lens ($f_1 = 25$ mm, $f_2 = 150$ mm, $f_3 = 200$ mm, and $f_4 = 200$ mm); M, mirror; LCD, liquid-crystal display; O, objective; PM, pop-up mirror; CCD, CCD camera. The objective, O_2, was placed at the focus (or Fourier plane) of lens L_4. The corresponding optical fields or holograms are represented at the appropriate planes.

slit, which we do not want to transmit any light, is encoded with a "checkerboard" pattern. By assigning alternating sets of pixels on LCD_1 with phase values that are out of phase by π, the light reflected from the LCD is scattered from its initial propagation axis [30–32].

A. Symmetric Superposition of Two Bessel Beams

The first three digital holograms, represented in the first column of Fig. 3, consist of a ring slit separated into two ring slits possessing azimuthal phases of equal order but opposite handedness (i.e., $l_{\text{inner}} = 3$ and $l_{\text{outer}} = -3$). However, the widths of the two ring slits differ in Figs. 3(d) and 3(g). This allowed us to control the weighting of the two Bessel beams and subsequently set the values of A_0 and α_0 in Eq. (1). The dimensions (in pixels) of the ring slits in Fig. 3 are (a) $r_1 = 173$, $r_2 = 188$, Δr_1, $\Delta r_2 = 15$; (d) $r_1 = 173$, $r_2 = 188$, $\Delta r_1 = 7$, $\Delta r_2 = 23$; (g) $r_1 = 173$, $r_2 = 188$, $\Delta r_1 = 23$, $\Delta r_2 = 7$. In the case that LCD_1 was encoded with two ring slits where the orders of the two azimuthal phases were of equal but opposite handedness, a "petal" structure was produced, where the number of "petals" is denoted by $2|l|$ [Figs. 3(b) and 3(c)], as expected from theory [28]. In the following two cases [Figs. 3(d) and 3(g)], the two ring slits had slightly different areas, resulting in the energy contained in the two Bessel beams being of slightly different weightings. In Figs. 3(e) and 3(f), the $l = -3$ order Bessel beam is heavily weighted by increasing the area of the outer ring slit, giving rise to a "smearing" of the "petals" as the $l = -3$ order Bessel beam dominants the optical field. Similarly, this is also evident in the case of Figs. 3(h) and 3(i), where the $l = 3$ order Bessel beam is heavily weighted by increasing the area of the inner ring slit.

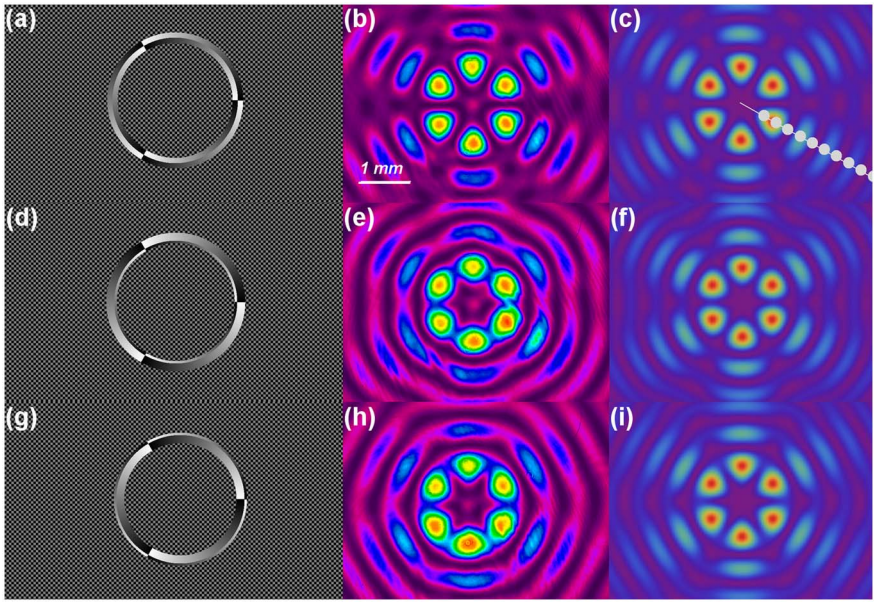

Fig. 3. (Color online) Digital ring slits [first column—(a), (d), (g)] and the corresponding experimentally produced fields in the Fourier plane [second column—(b), (e), (h)] accompanied by theoretically calculated fields [third column—(c), (f), (i)]. The ten white dots in (c) denote the radial positions of each of the ten ring slits used in the match filters.

The resulting superposition field, formed at the focal plane of L_3, was magnified with a 10× objective, O_1, and directed to the LCD of the second SLM, LCD_2. A pop-up mirror, PM_1, was used to direct the field at the plane of LCD_2 so as to be recorded on CCD_1 (Spiricon, LBA-FW-SCOR-7350115), so that the radial positions within the optical field could be quantitatively measured. LCD_2, programmed with a match filter, $\exp(-in\theta)$, together with lens L_4, was used to perform the inner product of the incoming field with the match filter given in Eq. (7). The match filter, also programmed as a digital hologram, consists of a single ring slit which also makes use of the "checkerboard" pattern. Since the match filter is programmed digitally, the radius of the ring slit, as well as the azimuthal phase within the ring slit, can be easily varied. This dynamical aspect of the SLM allows us to radially locate where in the optical field we wish to make a measurement of the OAM density. In this paper, the match filters consist of ring slits having 10 different radii [$r_1 = 75$, $r_2 = 110$, $r_3 = 145$, $r_4 = 180$, $r_5 = 215$, $r_6 = 250$, $r_7 = 285$, $r_8 = 320$, $r_9 = 355$, and $r_{10} = 390$ (given in pixels), each consisting of a width of 20 pixels], where the phase within the rings, n, varied as the complex conjugate of the azimuthal modes present in the incoming optical field. The location of the ten radial positions in the optical field is illustrated in Fig. 3(c). Because LCD_2 was orientated as the mirror image of LCD_1 in our experimental setup, the complex conjugate of the azimuthal mode index, n, on LCD_1 is equivalent to n on LCD_2. If the reader wishes to orientate the experimental setup differently, such that the two SLMs have the same orientation (i.e., are not mirror images of each other), the complex conjugate of the azimuthal mode index, n, on LCD_1 is then equivalent to $-n$ on LCD_2. The OAM density for a particular radial position can then be measured directly from Eqs. (15) and (24) by measuring the on-axis intensity of the inner product.

In determining the OAM density for the first three optical fields, denoted experimentally in the second column of Fig. 3, the intensity at the origin of the resulting field at the Fourier plane of L_4 was measured with a CCD camera, CCD_2, for each of the match filters and substituted into Eq. (15) or (24). The measured OAM densities as a function of the radial position for the first three optical fields are given in Fig. 4.

In Fig. 4(a), since the incoming optical field consists of an equal weighting of $l_{\text{inner}} = 3$ and $l_{\text{outer}} = -3$ order Bessel beams [Fig. 3(b)], the OAM density represented in the x–y plane consists of evenly sized concentric rings of positive and negative OAM. This is also evident in the radial cross-sectional profile of the OAM density in Fig. 4(b). The OAM density oscillates evenly around a value of zero. In the following two cases, where $l_{\text{inner}} = -3(+3)$ is heavily weighted, the OAM is predominantly negative (positive) and is evident in Fig. 4(d) [(f)]. This is also evident in Fig. 4(c) [(e)], where the OAM density exists predominantly in the negative (positive) quadrant of the graph.

A theoretical error band for the OAM density was obtained by determining the minimum and maximum values for the OAM density when the inner and outer radii of the ring slit in the match filters were displaced by half the width of the ring slit (i.e., 10 pixels). The error is so small that the error bands lie on top of one another and are not evident in the graphs. The experimental x error bar is given by a displacement of the ring slit in the match filter by half of its width, and so the absolute x error is 80 um (10 pixels × 8 um). We narrowed the error in experimentally measuring the on-axis intensity of the inner product to three factors: (1) human error in selecting the on-axis intensity of the inner product on CCD_2, (2) the positioning of CCD_2 in the Fourier pane of L_4, and (3) an adjustment of the ring slit (by half of its width) in the match filter on LCD_2. An aperture having a diameter of 10 pixels was positioned around the on-axis intensity on CCD_2, and the percentage error for the total energy within the aperture when it was moved 7 pixels from the center was included in the experimental error for the OAM density. The second error measurement involved measuring the percentage error for the on-axis intensity when CCD_2 was positioned 1 mm before and 1 mm after the Fourier plane of L_4. Finally, the last error measurement in the OAM density involved measuring the percentage error in the measured intensity when the radius of the ring slit on LCD_2 was either decreased or increased by half of the ring slit width. All of these aforementioned errors were measured and included in all the measurements.

B. Nonsymmetric Superposition of Two Bessel Beams

The fourth digital ring slit [Fig. 5(a)] consists of two ring slits having azimuthal phases $l_{\text{inner}} = 3$ and $l_{\text{outer}} = -4$, which is an example of a nonsymmetric superposition [described mathematically in Eq. (19)]. The dimensions (in pixels) of the ring slits in Fig. 5(a) are $r_1 = 173$, $r_2 = 188$, Δr_1, and $\Delta r_2 = 15$. The field produced [Fig. 5(b)] is in good agreement with the theoretically calculated field [Fig. 5(c)] and consists of a "petal" structure, where the number of "petals" is given by $|l_{\text{inner}}| + |l_{\text{outer}}|$, (i.e., 7 petals, for this case). The field has a global OAM of $-1\hbar$ ($3\hbar + -4\hbar$), and therefore the OAM density is mostly negative radially across the field, as is evident in both Figs. 5(d) and 5(e). In a nonsymmetric superposition, the OAM density is not symmetric in the optical field, as is evident in Fig. 5(e). Since the OAM density is not uniform in all radial directions of the optical field, the OAM density plotted in Fig. 5(d) is not for a particular angular point in the optical field, but instead an average over all angular positions.

C. Nonsymmetric Superposition of Three Bessel Beams

The fifth digital hologram [Fig. 6(a)] is divided into three ring slits having the following azimuthal phase variations: $l_{\text{inner}} = -3$, $l_{\text{middle}} = 2$, $l_{\text{outer}} = 1$,

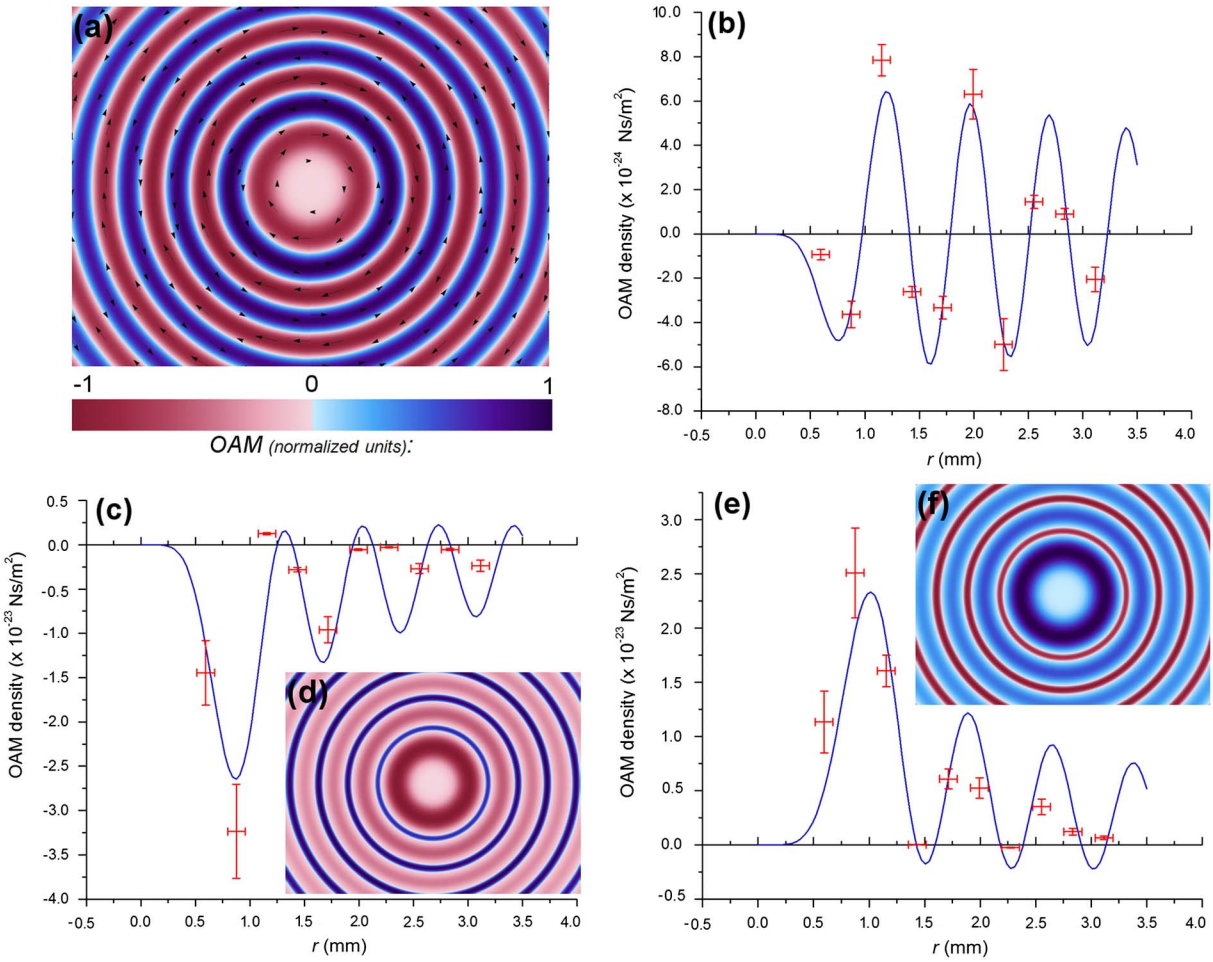

Fig. 4. (Color online) (a) Density plot of the OAM density for the field given in Fig. 3(b). Red denotes negative OAM, and blue denotes positive. Light to dark blue denotes an increase in positive OAM, and light to dark red denotes an increase in negative OAM. (b), (c), (e), The theoretical (blue curve) and experimentally measured (red points) OAM density for the corresponding fields in Figs 3(b), 3(e), and 3(h), respectively. (d), (f), Plots of the OAM density for (c) and (e), respectively, given as insets.

producing a nonsymmetric superposition. The dimensions (in pixels) of the ring slits in Fig. 6(a) are $r_1 = 170$, $r_2 = 180$, $r_3 = 190$, Δr_1, Δr_2, and $\Delta r_3 = 10$. Even though one cannot intuitively predict how the field will manifest in the Fourier plane, our experimental field [Fig. 6(b)] is in very good

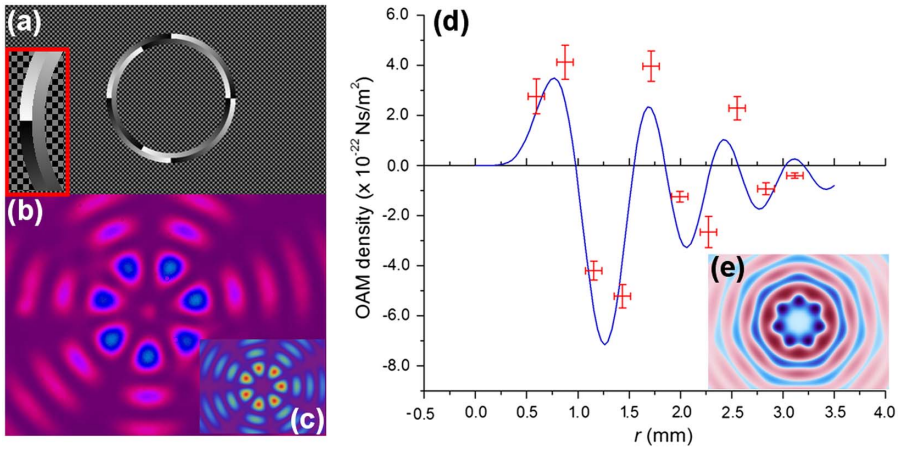

Fig. 5. (Color online) (a) Digital hologram used to generate (b) the experimental field; (c) the theoretical field. A magnification of the ring slit is given as an inset in (a). (d) The theoretical (blue curve) and experimentally measured (red points) OAM density. (e) A plot of the OAM density. Red denotes negative OAM, and blue denotes positive. Light to dark blue denotes an increase in positive OAM, and light to dark red denotes an increase in negative OAM.

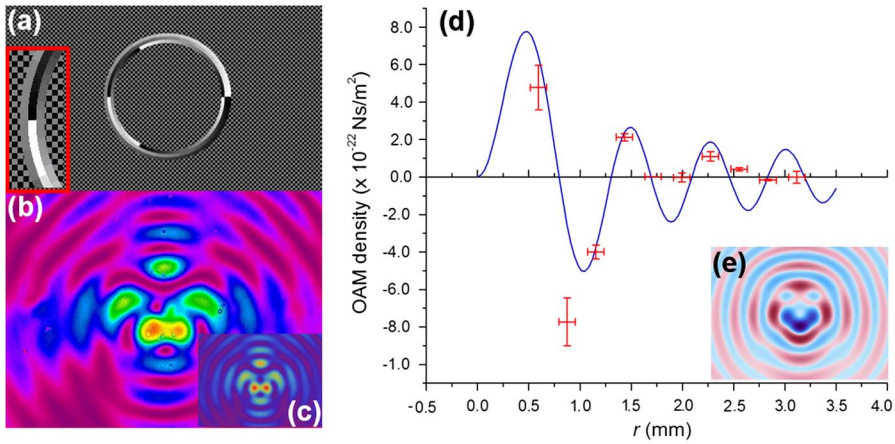

Fig. 6. (Color online) (a) Digital hologram used to generate (b) the experimental field; (c) the theoretical field. A magnification of the ring slit is given as an inset in (a). (d) The theoretical (blue curve) and experimentally measured (red points) OAM density. (e) A plot of the OAM density. Red denotes negative OAM, and blue denotes positive. Light to dark blue denotes an increase in positive OAM, and light to dark red denotes an increase in negative OAM.

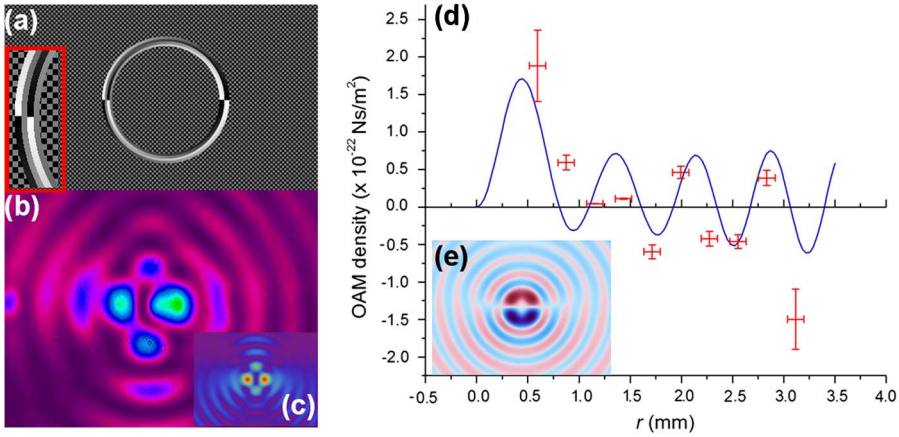

Fig. 7. (Color online) (a) Digital hologram used to generate (b) the experimental field; (c) the theoretical field. A magnification of the ring slit is given as an inset in (a). (d) The theoretical (blue curve) and experimentally measured (red points) OAM density. (e) A plot of the OAM density. Red denotes negative OAM, and blue denotes positive. Light to dark blue denotes an increase in positive OAM, and light to dark red denotes an increase in negative OAM.

agreement with the theoretically calculated field [Fig. 6(c)]. Since the ring slits are equally weighted and the azimuthal mode indices of the ring slits [Fig. 6(a)] sum to zero, the global OAM is zero, giving rise to the OAM density existing equally in both the negative and positive quadrants for the OAM density across the radial direction of the field, as is evident in Figs. 6(d) and 6(e). The OAM density is not uniform in all radial directions of the optical field [evident in Fig. 6(e)], and so the OAM density plotted in Fig. 6(d) is an average over all angular positions.

D. Nonsymmetric Superposition of Four Bessel Beams

A similar behavior is noted in the last optical field, whose digital hologram is depicted in Fig. 7(a). The ring slits have the following azimuthal mode indices: $l_{\text{inner}} = -2$, $l_{\text{middle}} = -1$, $1_{\text{middle2}} = 2$, $l_{\text{outer}} = 1$, which too sum to zero, and the physical dimensions (in pixels) are $r_1 = 169$, $r_2 = 176$, $r_3 = 183$, $r_4 = 190$, Δr_1, Δr_2, Δr_3, and $\Delta r_4 = 7$. Since the global OAM is zero, the OAM density exists equally in both the negative and positive quadrants, as is evident in Figs. 7(d) and 7(e). Once again, the OAM density is not uniform in all radial directions of the optical field [evident in Fig. 7(e)], and so the OAM density plotted in Fig. 7(d) is an average over all angular positions.

For the six cases presented above, the on-axis intensity recorded at CCD_2 for each of the match filters (varying in ring slit radius and azimuthal order) was measured and analyzed using the results obtained from Eqs. (4) and (5). From all six plots, it is evident that there is very good agreement between the experimentally measured OAM density values and those calculated theoretically. For the first time, to the best of our knowledge, the OAM density has been measured as a quantitative value and represented as the angular momentum per unit volume, Ns/m^2, by implementing an extremely simple measurement technique.

4. Conclusion

We have derived expressions for the OAM density for symmetric and nonsymmetric optical fields theoretically and made a direct comparison experimentally.

A simple technique for making such measurements of the OAM density in optical fields is tested on superimposed nondiffracting higher-order Bessel beams. However, the presented measurement technique can be used on any optical field carrying OAM. We obtain quantitative measurements, expressed as the angular momentum per unit volume, $\mathrm{Ns/m^2}$, for the OAM density as a function of the radial position in both symmetric and nonsymmetric optical fields, illustrating good agreement with the theoretical prediction. We find that the OAM density can be made to oscillate from positive to negative by appropriately adjusting the widths of the ring slits or the azimuthal orders within the ring slits, making it an ideal tool in the field of optical trapping and tweezing. Measuring the OAM spectrum of fields has direct relevance in the optical control of flow in microfluidic devices and in constructing optically driven micromachines and parallel molecular or cell assays.

Appendix A

The following proof illustrates that the ϕ-component of the Poynting vector, S_ϕ, is a linear operator. We start with the equation for S_ϕ:

$$S_\phi = \frac{\varepsilon_0 \omega c^2 i}{4}(u\nabla u^* - u^*\nabla u), \tag{A1}$$

where u is the optical field described in Eq. (1).

u^* can be written in terms of u as follows:

$$\begin{aligned} u + u^* &= A_0(J_l \exp(i\Delta kz)\exp(il\theta) \\ &\quad + \alpha_0 J_{-l} \exp(-i\Delta kz)\exp(-il\theta)) \\ &\quad + A_0(J_l \exp(-i\Delta kz)\exp(-il\theta) \\ &\quad + \alpha_0 J_{-l} \exp(i\Delta kz)\exp(il\theta)) \\ u + u^* &= (A_0 J_l + A_0\alpha_0 J_{-l})2\cos(\Delta kz + l\theta) \\ \rightarrow u^* &= \underbrace{2A_0(J_l + \alpha_0 J_{-l})\cos(\Delta kz + l\theta)}_{X} - u, \end{aligned} \tag{A2}$$

where for convenience we have left the terms not involving u as X.

Substituting u^* into Eq. (A1) results in

$$\begin{aligned} S_\phi &\propto u\nabla u^* - u^*\nabla u \propto u\nabla(X-u) - (X-u)\nabla u \\ &\propto u\nabla X - u\nabla u - X\nabla u + u\nabla u \propto u\nabla X - X\nabla u, \end{aligned} \tag{A3}$$

which is a linear operator, i.e., $S_\phi(u_1 + u_2) = S_\phi(u_1) + S_\phi(u_2)$. Thus, the linear momentum (in the azimuthal coordinate) from the Poynting vector of a sum of fields is equal to the sum of the linear momentums of each individual field.

References

1. L. Allen, M. W. Beijersbergen, R. J. C. Spreeuw, and J. P. Woerdman, "Orbital angular momentum of light and the transformation of Laguerre-Gaussian laser modes," Phys. Rev. A **45**, 8185–8189 (1992).
2. H. He, M. E. J. Friese, N. R. Heckenberg, and H. Rubinsztein-Dunlop, "Direct observation of transfer of angular momentum to absorptive particles from a laser beam with a phase singularity," Phys. Rev. Lett. **75**, 826–829 (1995).
3. A. Mair, A. Vaziri, G. Weihs, and A. Zeilinger, "Entanglement of the orbital angular momentum states of photons," Nature **412**, 313–316 (2001).
4. M. W. Beijersbergen, L. Allen, H. E. L. O. Van der Veen, and J. P. Woerdman, "Astigmatic laser mode converters and the transfer of orbital angular momentum," Opt. Commun. **96**, 123–132 (1993).
5. Arlt and K. Dholakia, "Generation of high-order Bessel beams by use of an axicon," Opt. Commun. **177**, 297–301 (2000).
6. H. I. Sztul and R. R. Alfano, "The Poynting vector and angular momentum of Airy beams," Opt. Express **16**, 9411–9416 (2008).
7. A. Vaziri, G. Weihs, and A. Zeilinger, "Experimental two-photon three-dimensional quantum entanglement," Phys. Rev. Lett. **89**, 240401 (2002).
8. J. T. Barreiro, T.-C. Wei, and P. G. Kwiat, "Beating the channel capacity limit for linear photonic superdense coding," Nat. Phys. **4**, 282–286 (2008).
9. J. Leach, B. Jack, J. Romero, A. K. Jha, A. M. Yao, S. Franke-Arnold, D. Ireland, R. W. Boyd, S. M. Barnett, and M. J. Padgett, "Quantum correlations in optical angle-orbital angular momentum variables," Science **329**, 662–665 (2010).
10. G. Gibson, J. Courtial, M. J. Padgett, M. Vasnetsov, V. Pas'ko, S. M. Barnett, and S. Franke-Arnold, "Free-space information transfer using light beams carrying orbital angular momentum," Opt. Express **12**, 5448–5456 (2004).
11. S. N. Khonina, V. V. Kotlyar, R. V. Skidanov, V. A. Soifer, P. Laakkonen, and J. Turunen, "Gauss–Laguerre modes with different indices in prescribed diffraction orders of a diffractive phase element," Opt. Commun. **175**, 301–308 (2000).
12. G. C. G. Berkhout, M. P. J. Lavery, J. Courtial, M. W. Beijersbergen, and M. J. Padgett, "Efficient sorting of orbital angular momentum states of light," Phys. Rev. Lett. **105**, 153601 (2010).
13. J. Leach, M. J. Padgett, S. M. Barnett, S. Franke-Arnold, and J. Courtial, "Measuring the orbital angular momentum of a single photon," Phys. Rev. Lett. **88**, 257901 (2002).
14. M. Lavery, A. Dudley, A. Forbes, J. Courtial, and M. Padgett, "Robust interferometer for the routing of light beams carrying orbital angular momentum," New J. Phys. **13**, 093014 (2011).
15. C. Gao, X. Qi, Y. Liu, J. Xin, and L. Wang, "Sorting and detecting orbital angular momentum states by using a Dove prism embedded Mach–Zehnder interferometer and amplitude gratings," Opt. Commun. **284**, 48–51 (2011).
16. A. Gatto, M. Tacca, P. Martelli, P. Boffi, and M. Martinelli, "Free-space orbital angular momentum division multiplexing with Bessel beams," J. Opt. **13**, 064018 (2011).
17. J. M. Hickmann, E. J. S. Fonseca, W. C. Soares, and S. Chavez-Cerda, "Angular Momentum," Phys. Rev. Lett. **105**, 053904 (2010).
18. V. Garces-Chavez, D. McGloin, M. J. Padgett, W. Dultz, H. Schmitzer, and K. Dholakia, "Observation of the transfer of the local angular momentum density of a multiringed light beam to an optically trapped particle," Phys. Rev. Lett. **91**, 093602 (2003).
19. C. H. J. Schmitz, K. Uhrig, J. P. Spatz, and J. E. Curtis, "Tuning the orbital angular momentum in optical vortex beams," Opt. Express **14**, 6604–6612 (2006).
20. S. H. Tao, X. C. Yuan, J. Lin, and R. E. Burge, "Residue orbital angular momentum in interferenced double vortex beams with unequal topological charges," Opt. Express **14**, 535–541 (2006).
21. K. Volke-Sepulveda, V. Garces-Chavez, S. Chavez-Cerda, J. Arlt, and K. Dholakia, "Orbital angular momentum of a high-order Bessel light beam," J. Opt. B: Quantum Semiclass. Opt. **4**, S82–S89 (2002).
22. V. Garces-Chavez, K. Volke-Sepulveda, S. Chavez-Cerda, W. Sibbett, and K. Dholakia, "Transfer of orbital angular momentum to an optically trapped low-index particle," Phys. Rev. A **66**, 063402 (2002).

23. M. V. Vasnetsov, J. P. Torres, D. V. Petrov, and L. Torner, "Observation of the orbital angular momentum spectrum of a light beam," Opt. Lett. **28**, 2285–2287 (2003).
24. M. Hautakorpi, J. Lindberg, T. Setälä, and M. Kaivola, "Rotational frequency shifts in partially coherent optical fields," J. Opt. Soc. Am. A **23**, 1159–1163 (2006).
25. X. Gan, P. Zhang, S. Liu, Y. Zheng, J. Zhao, and Z. Chen, "Stabilization and breakup of optical vortices in presence of hybrid nonlinearity," Opt. Express **17**, 23130–23136 (2009).
26. I. Litvin, A. Dudley, and A. Forbes, "Poynting vector and orbital angular momentum density of superpositions of Bessel beams," Opt. Express **19**, 16760–16771 (2011).
27. J. Durnin, J. Miceli Jr., and J. H. Eberly, "Diffraction-free beams," Phys. Rev. Lett. **58**, 1499–1501 (1987).
28. R. Vasilyeu, A. Dudley, N. Khilo, and A. Forbes, "Generating superpositions of higher-order Bessel beams," Opt. Express **17**, 23389–23395 (2009).
29. A. V. Lugt, "Signal detection by complex spatial filtering," IEEE Trans. Inf. Theory **10**, 139–145 (1964).
30. D. W. K. Wong and G. Chen, "Redistribution of the zero order by the use of a phase checkerboard pattern in computer generated holograms," Appl. Opt. **47**, 602–610 (2008).
31. C. Lopez-Mariscal and K. Helmerson, "Shaped nondiffracting beams," Opt. Lett. **35**, 1215–1217 (2010).
32. A. Dudley, R. Vasilyeu, V. Belyi, N. Khilo, P. Ropot, and A. Forbes, "Controlling the evolution of nondiffracting speckle by complex amplitude modulation on a phase-only spatial light modulator," Opt. Commun. **285**, 5–12 (2012).